

AO09: Retrieving the complex refractive index of volcanic ash for wavelengths in the visible spectrum

Supervisors: Dr R. G. Grainger & B. E. Reed

To fully exploit the remote sensing technologies that are used to monitor a volcanic eruption and return information on its plume, the complex refractive index of the ingredient volcanic ash is required. This report presents how the complex refractive index was determined for a set of volcanic ash samples taken from various sources, for light at three visible wavelengths (450.0 nm, 546.7 nm and 650.0 nm). With the use of an optical microscope, the Becke line method was employed to acquire the real part of the refractive index of ash samples taken from eruptions at Grímsvötn (Iceland), Chaitén (Chile), Etna (Italy), Eyjafjallajökull (Iceland), Tongariro (New Zealand), Askja (Iceland), Nisyros (Greece), Okmok (Alaska), Augustine (Alaska) and Spurr (Alaska). An original method involving the digital analysis of microscopic images of the constituent ash particles was used to derive the imaginary part of the refractive index of ash samples taken from Grímsvötn, Chaitén, Eyjafjallajökull, Tongariro, Nisyros and Okmok.

1 Introduction

A volcanic eruption has the potential to pose a variety of severe and widespread threats to human well-being. Beyond the obvious calamitous effects to anyone in the immediate vicinity, eruptions are also known to cause acute respiratory difficulties to people unfortunate enough to be caught in an ash fall [1]. Furthermore, it is well documented that the resulting injection of aerosols into the atmosphere is a hazard to civil aviation [2], as well as the cause of dramatic climatic events [3]. It is imperative therefore, that we can effectively monitor these imposing and destructive events.

One way to acquire information on an eruption is through remote sensing, particularly satellite observation. Images taken from space can cover vast areas and so are able to provide a complete view of an ash cloud. However, an unfortunate fact of remote sensing is that properties of the target are often required before accurate measurements can be taken. To acquire detailed information on a plume, *a priori* information on the size, shape and optical properties of the constituent matter is needed [4].

Volcanic ash is defined as being pyroclasts with a diameter of less than 2 mm. The content of vol-

canic ash depends entirely upon the eruptive processes in engagement at the time of production, but generally it can be said to be made up of a mixture of vitric (glass), crystalline and lithic (rock) particles [5]. Volcanic glass is formed from fragments of magma which have cooled and solidified during the progression of an eruption. Crystalline material grows in the magma beneath the Earth before it is expelled. The rock fragments are present as a result of being broken off the walls of the magma conduit by the force of the eruptive flow [6]. The myriad of different particles means that understanding the overall optical effect of volcanic ash is particularly challenging.

The complex refractive index ($m = n + ik$) of a substance provides information on how it scatters and absorbs radiation but existing measurements of this parameter for volcanic ash are very limited. Papers by Patterson give only values of the imaginary part of ash from eruptions at Mt. St. Helens [7], El Chichón [8] (both in the spectral range 0.3-0.7 μm) and Mayon [9] (in the spectral range 1-16 μm). Krotkov et al. (1999) were able to determine both the real and imaginary parts for ash from Mt. Spurr at three frequencies in the ultraviolet spec-

tral region [10]. Recent progress has been made by Grainger et al. (2013) who were able to retrieve the real and imaginary parts for ash from the 1993 eruption of Mt. Aso in the spectral range 1-20 μm [4]. More values of the refractive indices of volcanic material including basalt [11, 12], andesite [11, 12], pumice [13], obsidian [11] and granite [14] are available. However, these can only ever provide an approximation to real ash. To be able to make maximum use of satellite imagery and modern precision instruments, the refractive indices of a range of ashes needs to be determined.

Observing a volcanic plume via satellite is possible as it perturbs the Earth's radiation field through absorption and scattering of radiation. Transmission through an optically active medium is related to its physical properties via Bourguer's Law [15]:

$$\mathcal{T}(\lambda) = e^{-\beta_{ext}(\lambda)x} \quad (1)$$

where β_{ext} is the volume extinction coefficient. According to Mie theory, it is given by [16]:

$$\beta_{ext} = \int_0^{\infty} Q_{ext}(r, m(\lambda), \lambda) \pi r^2 n(r) dr \quad (2)$$

where Q_{ext} is the extinction efficiency, which can be calculated with Mie theory from values for the particle radius, wavelength of light and the complex refractive index. The variable $n(r)$ is the number of particles with a given radius and is often assumed to conform to a log-normal distribution in the case of volcanic ash [4]. With knowledge of the complex refractive index of ash we gain the ability to calculate the extinction coefficient and therefore an understanding of how radiation is attenuated as it passes up from the Earth, through an ash cloud and up to a satellite. For visible light, the relative levels of back scattered light can also be important. Instruments on board a satellite can measure such perturbations in intensity, so by comparing this to the Earth's unperturbed field, defining features of the volcanic plume can be determined. One such feature is mass loading (concentration of ash) which is important when determining whether a region is safe for a plane to fly through. Francis, Cook and Sanders (2012) describe how they retrieved the physical properties of ash from the 2010 Eyjafjallajökull eruption using data from the Meteosat weather satellite, noting their results were very sensitive to the choice of the assumed

refractive indices [17]. Without the availability of a refractive index specific to the ash, they settled on the very general values of andesite [11], a fact which highlights the relevance and importance of this project.

In the following report, an account of the methods used to retrieve the complex refractive index for a set of volcanic ash samples is presented. An application of the Becke line method was used to retrieve an overall value of the real part of the refractive index for ten ash samples. This method required an optical microscope to inspect the signature movements of light, caused by refraction and internal reflection, produced when the ash particles were immersed in a medium of a known refractive index and illuminated from below. An original method, involving the measurement and combination of the imaginary part for individual particles within a sample, was used to calculate an overall value of the imaginary part of the refractive index for six of the ash samples. This method involved taking microscopic photographs of the ash samples, and digitally analysing them to determine the levels of light absorption occurring in the individual particles. The overall value of the imaginary part of the refractive index of a sample was found from the absorptive effects of the constituent particles by volume-averaging. A list of the ashes investigated is provided in Table 1, along with the reference numbers by which the samples will be referred to throughout.

Ref.	Source	Date
VA5	Grímsvötn, Iceland	22-25/5/2011
VA11	Chaitén, Chile	2008
VA10	Etna, Italy	1/7/2001
VA15	Eyjafjallajökull, Iceland	15-16/5/2010
VA16	Tongariro, New Zealand	2012
VA17	Askja, Iceland	1875
VA19	Nisyros, Greece	Unknown
VA20	Okmok, Alaska	July 2008
VA21	Augustine, Alaska	13/01/2006
VA22	Spurr, Alaska	August 1992

Table 1: Reference table showing the reference numbers, eruption sources and dates of the volcanic ash specimens which were examined.

2 Background

2.1 The complex refractive index

The complex refractive index, m , describes how light propagates in a medium and can be expressed as:

$$m = n + ik \quad (3)$$

A plane wave travelling in an homogeneous medium with this refractive index may be described in the form [15]:

$$\mathbf{E} = \mathbf{E}_0 \exp\left(-\frac{2\pi kz}{\lambda}\right) \exp\left(\frac{i2\pi nz}{\lambda} - i\omega t\right) \quad (4)$$

where \mathbf{E} is the electric field, \mathbf{E}_0 is the electric field at $z = 0$, λ is the wavelength of light *in vacuo* and ω is the angular frequency of the light. From this, it follows that k , the imaginary part of the refractive index, determines the attenuation of wave as it travels through the medium. The real part of the refractive index determines the phase velocity, $v = c/n$, therefore describing how light is refracted when entering the medium. From this, the Poynting vector, $\mathbf{S} = \mathbf{E} \times \mathbf{H}$, can be shown to be [15]:

$$\mathbf{S} = \frac{1}{2} \text{Re} \left\{ \sqrt{\frac{\epsilon}{\mu}} \right\} |\mathbf{E}_0|^2 \exp\left(-\frac{4\pi kz}{\lambda}\right) \hat{\mathbf{e}} \quad (5)$$

where $\hat{\mathbf{e}}$ is the unit vector in the direction of wave propagation. The magnitude of \mathbf{S} is called the irradiance, I . As the wave progresses through the medium without scattering, the irradiance is exponentially diminished as described by the Beer-Lambert law [15]:

$$I = I_0 e^{-\beta_{abs} z} \quad (6)$$

where the absorption coefficient is given by:

$$\beta_{abs} = \frac{4\pi k}{\lambda} \quad (7)$$

2.2 Absorption & scattering

When considering the absorption and scattering of light by a particle, the size of the particle relative to the wavelength of light is of fundamental significance. The regime in which an interaction is taking place is commonly expressed numerically as a dimensionless value called the size parameter, x :

$$x = \frac{2\pi a}{\lambda_1} \quad (8)$$

where a is the particle radius (for non-spherical particles the radius of a surface-equivalent sphere can be used) and λ_1 is the wavelength of light in the surrounding medium [18].

Rigorous treatment of the scattering of electromagnetic radiation by particles can be provided by Mie theory (for spherical particles) or the T-matrix method (for non-spherical particles). However, these techniques are mathematically laborious and require forward modelling of the system and so should be avoided where possible. In the limit where $x \rightarrow 0$, scattering becomes negligible and extinction can be said to be due entirely to absorption. This is known as the Rayleigh regime. On the other hand, as $x \rightarrow \infty$, geometric optics (ray tracing) becomes applicable [18].

Exactly how large or small the particles have to be in comparison to the incoming light for the above regimes to become good approximations is not entirely clear. In section 3.2, the method relies on the validity of the ray tracing approximation. Mishchenko, Travis and Lacis (2008) demonstrate that a reasonable match to Mie and T-matrix methods is achieved by the geometric optics approximation for size parameters of around 120 [18].

3 Project

3.1 Becke line method

The method used to retrieve the real part of refractive index was the Becke line test, which is based on the comparison of the mineral being studied to a mounting medium of a known refractive index.

3.1.1 Method outline

When a fragment of a mineral is immersed in a liquid of a different refractive index and illuminated from below, the effects of refraction and total internal reflection cause a concentrated band of light (known as the Becke line) to form close to the fragment-liquid interface. This rim of light is observable when such a fragment is viewed, slightly out of focus, under a microscope. If one were to start by viewing an immersed grain slightly above the focal point of the microscope's objective lens, and the stage were to be lowered (or equivalently, the focus raised) the Becke line would appear to

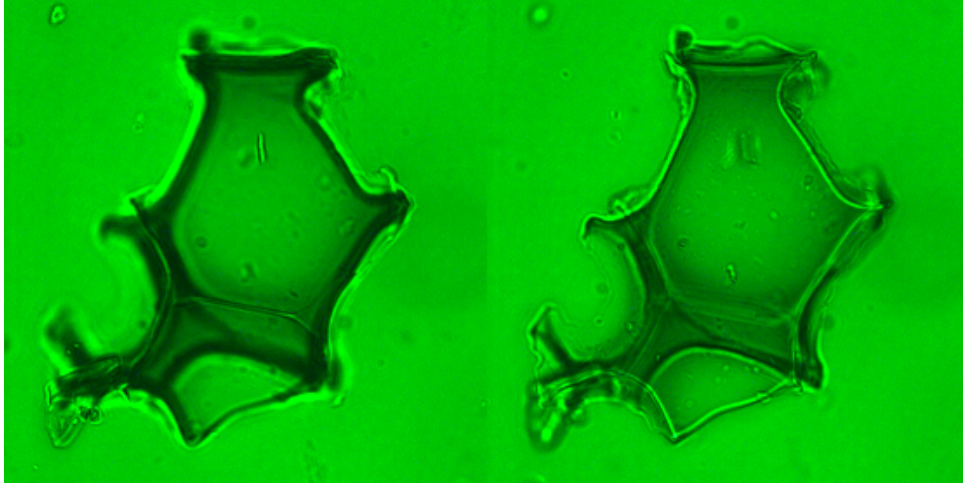


Figure 1: Ash fragment from the May 2011 eruption of Grímsvötn, Iceland immersed in liquid of refractive index $n = 1.55$ viewed at 546.7 nm. As the stage was lowered (left to right) the Becke line could be seen entering the fragment, demonstrating that the ash had a higher refractive index than the liquid at this wavelength.

move into the material with the higher refractive index. Nesse (1991) provides a detailed explanation as to why this happens [19]. Therefore, by immersing aerosol particles in a series liquids of known refractive index and observing in which direction the Becke line moves when the sample is brought through the focus, it is possible to deduce the refractive index of the aerosol particles themselves.

3.1.2 Experimental set-up

The ashes under investigation were compared to a set of Cargille Refractive Index Liquids. The set of nineteen liquids had a range of $n=1.4600$ to $n=1.6400$, separated by increments of 0.0100 (all with a standard error of ± 0.0002). The quoted refractive indices were for light of 589.3 nm wavelength at a temperature of 25°C. The Cauchy equations of the liquids were supplied by Cargille so their refractive indices could be calculated for different frequencies of light. The test was performed at three wavelengths: 450.0 nm, 546.7 nm and 650.0 nm. This was accomplished by placing optical filters, with a bandpass of ± 10 nm about the peak radiance, just above the objective lens of the microscope. About 3 mg of the ash was immersed in 50 μl of the $n = 1.50$ liquid and shaken up to disperse the fragments uniformly. This ratio ensured the fragments were well separated by the liquid, providing a clear view of the liquid-fragment boundaries. A couple of drops of the mixture were placed on a microscope slide and covered with a

cover slip. The slide was then placed on the microscope stage and illuminated from below by white light produced by a halogen lamp. One of the above listed filters was put in place. The sample was observed with a 20X objective through the microscope eyepiece as well as via a CCD digital camera linked up to a computer monitor. To maximise the contrast and depth of field, and thus produce the most well-defined Becke line possible, the aperture diaphragm was stopped down as much would still allow enough illumination for a clear image of the sample to be seen through the eyepiece [19].

The stage was repeatedly raised and lowered, moving the immersed ash particles through the microscope's focus. If the Becke lines moved from the fragments into the liquid as the stage was lowered, the ash was noted to have a refractive index lower than 1.50. In this case, a fresh batch of the ash would have been immersed in a liquid of a lower refractive index and the above process would have been repeated. If the Becke line moved from the liquid into the fragments, the ash was noted to have a higher refractive index than 1.50. In this case, a fresh batch of the ash would have been placed in a liquid of higher refractive index and the process would have been repeated. By repeating the process for successive liquids and recording whether the ash was of a refractive index which was higher or lower than the liquids it had been placed in, it was possible to hone in on a value for

the refractive index of the ash.

As the refractive index of the mount became more closely matched to the ash, the Becke lines became fainter. If an almost exact match was found, the Becke line would have been barely visible and the fragments would have appeared to blend with the surrounding mixture. If this was the case for all the particles in view, the ash would be assigned the same refractive index as that of the liquid. If all the Becke lines passed from the fragment into the liquid as the stage was lowered for one liquid, but passed from the liquid into the fragment when placed in the incrementally higher liquid, the ash was assigned the refractive index half way between the two liquids.

It was common to see Becke lines passing in opposite directions over the boundary, as well as some blending in for an ash in a specific liquid, indicating the presence of particles of varying refractive index. If this was the case a survey of 30 particles was taken and the number of particles going in each direction was counted and an average value was calculated. An example distribution is given in Table 2.

Liquid n	Number of particles		
	Into liquid	Blending	Into fragment
1.59	0	0	30
1.60	7	5	18
1.61	30	0	0

Table 2: The directions of the Becke line as the stage is lowered in an example ash sample immersed in liquids of refractive index 1.59-1.60.

For this example ash, it would be concluded that 7 particles have a refractive index of 1.595, 5 particles have a refractive index of 1.60 and 18 particles have a refractive index of 1.605. A weighted average of these would have been taken, and the ash would have been assigned a refractive index of 1.602. Of course, this value would have been corrected for the wavelength of light using the Cauchy equations of the liquids.

This method returned a value for the real part of the refractive index for all ten ash samples.

3.2 Particle absorption method

An original method to combine the individual absorption effects of the particles within the ash

samples to find an overall imaginary part of the refractive index was developed and implemented.

Prior knowledge of the value of the real part of the refractive index of each of the ash samples for 450.0 nm, 546.7 nm and 650.0 nm light was required for this method, hence why it was performed subsequent to the Becke line tests. Again, a wavelength to be studied was selected and the corresponding filter was placed above the objective lens of the microscope.

3.2.1 Method outline

The particles examined with this method had a typical surface-equivalent-sphere radius, r_s , between 15 μm and 35 μm . The wavelength of light in the medium, $\lambda_1 = \lambda_0/n$, ranged from 0.26 μm to 0.43 μm . Using Equation 8, the size parameter, x , was between 220 and 850. This meant that, according to the condition stated in Section 2.2, x was always large enough for the system to be adequately described in the geometric optics limit.

In the geometric optics approximation, the path of a ray between two mediums of different refractive index is governed by Snell's law:

$$n_2 \sin \theta_i = n_1 \sin \theta_t \quad (9)$$

where n_2 is the refractive index of the starting medium and n_1 is the refractive index of the medium to which the light is transmitted [15].

The refractive index of the liquid was approximately equal to the refractive index of the ash particles ($n_2 \simeq n_1$) meaning the angle of incidence and transmission were approximately equal and light was said to pass straight through the particle, without changing direction due to refraction. By this assumption, the intensity of light was not diminished due to scattering by the ash particles.

In geometric optics, the reflectance and transmittance at a plane boundary is governed by the Fresnel formulas. The formulas for the reflection coefficients of light where the electric vectors are parallel and perpendicular to the plane boundary are :

$$\tilde{r}_{\parallel} = \frac{\cos \theta_t - M \cos \theta_i}{\cos \theta_t + M \cos \theta_i} \quad (10)$$

$$\tilde{r}_{\perp} = \frac{\cos \theta_i - M \cos \theta_t}{\cos \theta_i + M \cos \theta_t} \quad (11)$$

where $M = m_1/m_2$ is the relative refractive index[15].

In the case of normally incident light travelling from a non-absorbing medium of $m_2 = n_2$ into an absorbing medium of $m_1 = n_1 + ik_1$ equations (10) and (11) can be reduced to the equation for the reflectance R for normally incident light:

$$R = |\tilde{r}|^2 = \frac{(n-1)^2 + k^2}{(n+1)^2 + k^2} \quad (12)$$

where $M = n + ik$ [15]. There are two important observations to be made using equation (12):

i. The reflectance at the slide-particle boundary was approximately equal to that of the slide-liquid boundary. This was because for light entering the particle or the liquid, n_1 was approximately equal and for the transparent mounting liquid $k_1 = 0$ and according to previous studies of volcanic ash at visible wavelengths, it should be possible to say that in the case of an ash particle $k_1 < 0.02$ [7, 8].

ii. The reflectance at the particle-liquid boundary was negligible as $n_1 \simeq n_2$.

Therefore, the path of light which travelled through the particle was essentially the same as the path of light travelling past the particles, apart from the absorption felt by the light which travelled through (as illustrated in Figure 2). This meant that the intensity of light leaving the particle had an intensity which had been reduced according to the Beer-Lambert law (Equation 6) relative to the light travelling past the particle.

By combining equations (6) and (7), an equation giving the imaginary part of the refractive index of the particle in terms of the intensity of light entering (I_0) and leaving (I_1) the particle was formulated:

$$k = \frac{\lambda}{4\pi d} \ln \left(\frac{I_0}{I_1} \right) \quad (13)$$

where d is the path length of the light in the particle.

As no light was absorbed by the mounting medium, the intensity of light entering the particle was equated to the intensity of the light passing through the slide unobstructed by ash particles.

3.2.2 Calibration of camera

The photographs taken from the CCD digital camera were stored as bitmap images, for which each pixel had an R, G and B (red, green and blue) coordinate, ranging from 0 to 255. These pixels values, as well as averages of the values over a specified region within an image, could be extracted

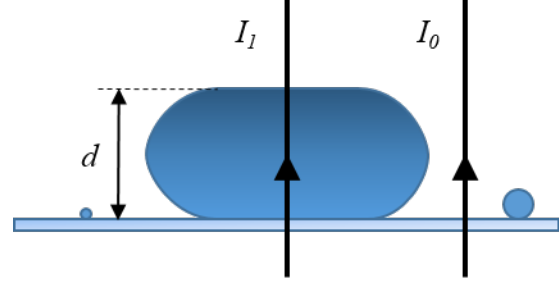


Figure 2: Diagram of two beams of light passing through the ash/liquid mixture. The beam labelled I_0 passes through unattenuated while the beam labelled I_1 is partially absorbed whilst travelling through the ash particle. The length d indicates the path length of the light in the particle.

from the image file using NI Vision Assistant software. To find out how transmittance could be related to the pixel parameters, neutral density filters of optical density $d = 0.3$ and $d = 0.6$ were used to provide known readings for of transmittance. The gamma correction and saturation of the camera were set to one¹. For each wavelength of light (again using the 450.0 nm, 546.7 nm and 650.0 nm filters), a set of 4 images was taken: one for the unobstructed stage (100% transmittance), one for each of the neutral density filters placed on the stage and one of the stage completely obstructed by a thick, opaque medium (0% transmittance).

The average RGB coordinates for a square region at the centre of these images was retrieved. For the images with the 650.0 nm filter in place, the average R coordinate was shown to have a linear relationship with fractional transmittance, with the intercept passing through the origin. The G and B coordinates did not register any significant value. Similarly, for 546.7 nm light, the G coordinate had a linear relationship with intensity, with the intercept passing through the origin without R or B registering, and for 450.0 nm light the B coordinate had a linear relationship with intensity, with the intercept passing through the origin. These calibration lines are shown in Appendix A.

Relative intensity could therefore be related to the relative pixel values by:

¹Gamma correction is a nonlinear operation applied to images to compensate for how humans perceive light intensity. Saturation describes the intensity of colour in an image. Setting these to 1 when taking photographs ensures the intensity dependent corrections to an image are minimised.

$$\frac{I_1}{I_0} = \frac{X_1}{X_0} \quad (14)$$

where X_0 and X_1 are the pixel coordinates for the unobstructed and attenuated light respectively. Substituting this into Equation 4 we get an equation for k in terms of the relevant pixel coordinates:

$$k = \frac{\lambda}{4\pi d} \ln \left(\frac{X_0}{X_1} \right) \quad (15)$$

where $X = R$ when 650.0 nm light was being observed, $X = G$ when 546.7 nm light was being observed, and $X = B$ when 450.0 nm light was being observed.

3.2.3 Measurements

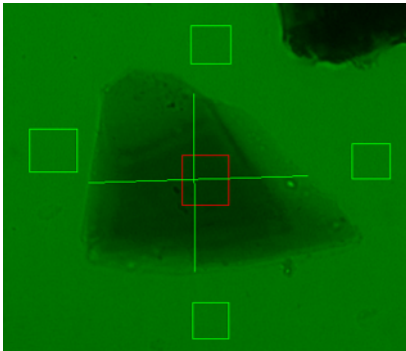


Figure 3: Illustration of the parameters extracted from the image of an ash particle. In this case, where $\lambda = 546.7\text{nm}$, the average G coordinate was extracted for a region at the centre of the particle as well as for four unobstructed regions surrounding the particle. The perpendicular width and breadth measurements are also shown.

Approximately 3 mg of ash was immersed in 60 μl of the mounting liquid with the closest matching refractive index at that wavelength. The mixture was shaken vigorously to disperse the ash and a few drops were placed on a microscope slide and covered with a cover slip. The sample was placed on the microscope stage and illuminated from below. An individual particle was selected and the stage was positioned so that it was at the focal point microscope's 20X objective lens.

Photographs were taken of the ash particle in the matched medium. For each fragment investigated, the average colour coordinate for an area at the centre of the ash fragment was measured and assigned to the variable X_1 . The average colour

coordinate for three or four unobstructed areas surrounding the fragment was also taken, then averaged and assigned to variable X_0 . By taking an average of multiple areas around the particle it reduced the chance of error caused by fluctuations in the illuminating field. The length (x_1) and breadth (x_2) of the particle were also extracted. A conversion between image pixels and microns was deduced by taking a photograph of a micro-ruler. An example of the extraction of these variables is shown in Figure 3.

The final value required to calculate k for the particle was the path length of the light as it travelled through the fragment. The relative vertical position of the base of the fragment was found by positioning the stage so that the microscope was focused on the upper surface of the glass slide. This position of the stage was read from the stage dial, which read to the nearest micron. The stage was then adjusted to focus on the upper surface at the centre of the fragment, visible due to the tiny imperfections which existed on the fragment's surface. The new position was read from the dial and its difference from the initial stage position was said to be the path length, d . The value of k was calculated and recorded for the particle. Lastly, the particle was assigned to a category of either clear (crystal or vitric), lithic (dark) or mixed. This process was repeated for 30 particles in each sample, at each wavelength of light.

3.2.4 Overall value from individual particles

To find a value for the imaginary part of the refractive index which is representative of the ash sample as a whole, an appropriate method of averaging the k values of the particles was needed. Due to effects such as fragmentation of the erupted particles, there was no guarantee that chemical composition and therefore k was independent of particle size [20].

According to Bohren and Huffman (1983), the factor $2a\beta_{abs}$ determines whether absorption is proportional to volume ($2a\beta_{abs} \ll 1$) or to area ($2a\beta_{abs} \gg 1$) [15]. In the case of the ashes under study, $2a\beta_{abs} \sim 1$ meaning that they were between the two regimes. However, in a similar study where Ebert et al. (2002) were aiming retrieving the overall complex refractive index from an ensemble of individual aerosol particles, it was found that volume-averaging the components of refractive index for the individual particles was in good agree-

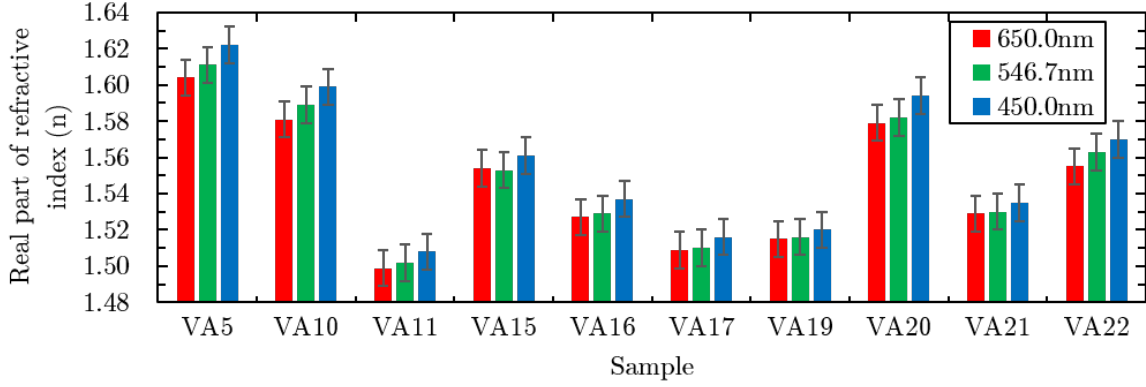


Figure 4: Chart showing the real part of refractive index at 650nm, 546.7nm and 450nm for 10 ash samples.

ment with overall photometer measurements [21].

Therefore, an effective imaginary part of the refractive index for the samples was calculated by taking a volume-weighted average of the k values of the individual particles:

$$k_{ash} = \frac{\sum_i V_i k_i}{\sum_j V_j} \quad (16)$$

where V_i is the volume of the individual particles. The exact morphology of the individual particles was not known. However, a particle could be modelled as an idealised cuboid or an idealised ellipsoid, and in both cases $V \propto x_1 x_2 d$. The fact that only the relative volume of the particles mattered, the product of the particle dimensions $x_1 x_2 d$ could be taken to be an approximate particle volume used to calculate the weights.

4 Results

4.1 Real part of the refractive index

A value for the mean real part of the refractive index was successfully retrieved at 450.0 nm, 546.7 nm and 650.0 nm for the 10 ash samples to an accuracy of ± 0.01 , determined by the resolution of mounting liquids. The values are presented in Figure 4 and quoted exactly in Table 3.

It can be seen in Figure 4 that the expected dispersion relation at visible wavelengths was evident in all samples, with the refractive index increasing with photon energy.

Ash Sample	Mean real refractive index (n)		
	650.0nm	546.7nm	450.0nm
VA5	1.604 ± 0.01	1.611 ± 0.01	1.622 ± 0.01
VA10	1.581 ± 0.01	1.589 ± 0.01	1.599 ± 0.01
VA11	1.499 ± 0.01	1.502 ± 0.01	1.508 ± 0.01
VA15	1.554 ± 0.01	1.553 ± 0.01	1.561 ± 0.01
VA16	1.527 ± 0.01	1.529 ± 0.01	1.537 ± 0.01
VA17	1.509 ± 0.01	1.510 ± 0.01	1.516 ± 0.01
VA19	1.515 ± 0.01	1.516 ± 0.01	1.520 ± 0.01
VA20	1.579 ± 0.01	1.582 ± 0.01	1.594 ± 0.01
VA21	1.529 ± 0.01	1.530 ± 0.01	1.535 ± 0.01
VA22	1.555 ± 0.01	1.563 ± 0.01	1.570 ± 0.01

Table 3: Table listing the real part of the refractive index for 10 ash samples at wavelengths of 650nm, 546.7nm and 450nm.

4.2 Imaginary part of the refractive index

The imaginary part of the refractive index was measured for 30 particles within six of the ash specimens at 450.0 nm, 546.7 nm and 650 nm. The distribution of the k values is shown in the form of histograms in Figure 5.

These histograms tend to show the k values conforming to a positively skewed distribution with the majority clustered around a modal peak and a long tail of outlying particles with much higher values of k . This clearly demonstrates the inhomogeneity in the particles present, with the lithic particles exhibiting unusually high absorption relative to the rest of the sample. Samples VA11, VA19 and VA5 even appear to show a secondary mode at substantially higher k values than the primary peak.

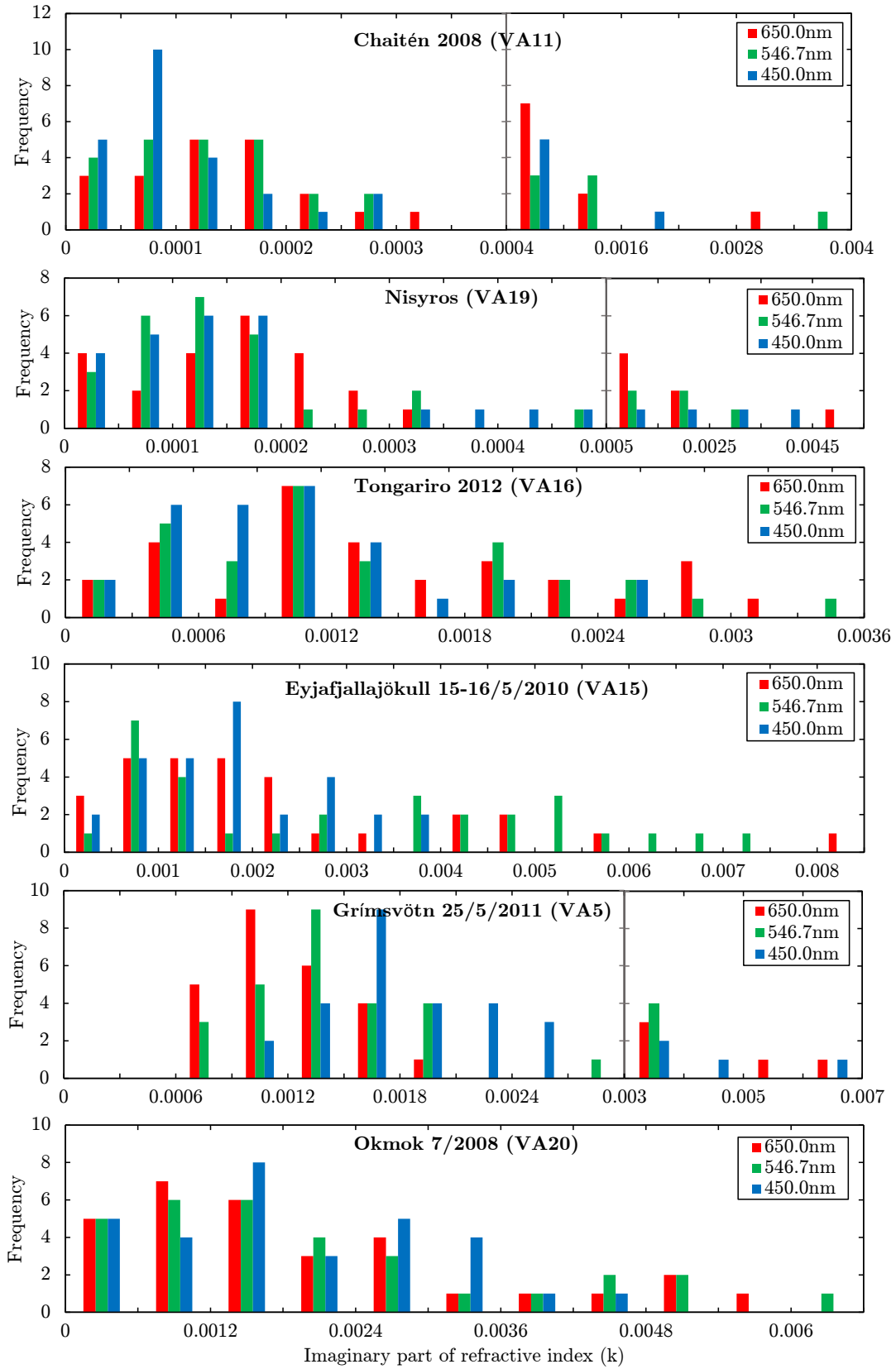


Figure 5: Combined histograms showing the distribution of k values amongst the 30 particles sampled from each specimen at 650.0 nm, 546.7 nm and 450.0 nm. There is a break in the x -axis showing a change in scale for (a), (b) and (e).

Ash Sample	Effective imaginary part of the refractive index (k)		
	650.0nm	546.7nm	450.0nm
VA11	0.000471 ± 0.00018	0.000508 ± 0.021	0.000314 ± 0.00012
VA19	0.000391 ± 0.00014	0.000325 ± 0.00021	0.000230 ± 0.00016
VA16	0.00107 ± 0.00028	0.00107 ± 0.00028	0.000696 ± 0.00024
VA15	0.000850 ± 0.00069	0.00108 ± 0.00058	0.000488 ± 0.00047
VA5	0.00129 ± 0.00017	0.00142 ± 0.00018	0.00155 ± 0.00027
VA20	0.00130 ± 0.00017	0.00145 ± 0.00023	0.00126 ± 0.000164

Table 4: Table listing the imaginary part of the refractive index at wavelengths of 650nm, 546.7nm and 450nm for six ash samples.

The overall imaginary refractive index values, calculated as a volume average of the sampled particles, are displayed in Figure 6 and quoted exactly in Table 4. The standard error was calculated by combining the weights from the averaging process with the standard deviations of the k values within the different particle categories, as detailed in Appendix B.

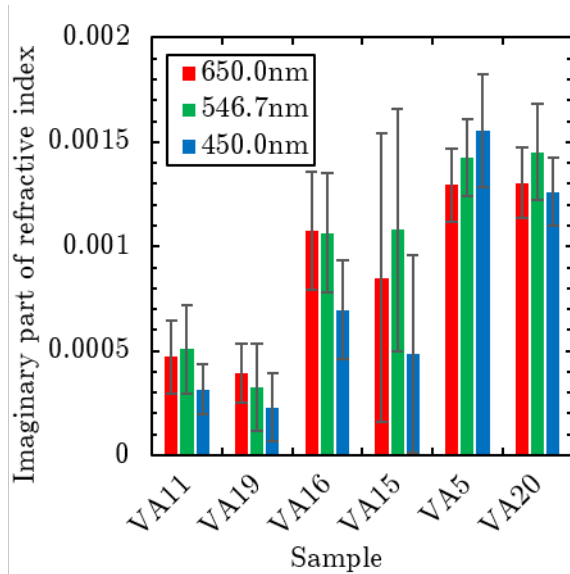


Figure 6: Chart showing the imaginary part of the refractive index at 650nm, 546.7nm and 450nm for 6 ash samples.

5 Discussion

The Becke line method is a standard procedure and returned good results. The resolution could have been increased had there been liquids of a finer refractive index incrementation. Furthermore, the inhomogeneity of particles could have been better accounted for. A similar volume-averaging tech-

nique to the one used in the method to find the imaginary part could have been used. However, the variation within a sample was generally small and embarking on the time consuming process of recording the volume and refractive index of each particle would not have been justified. The obvious dispersion relation, visible in all samples, provides reassurance and suggests that the errors attached to these results were in fact too cautious.

The particle absorption method seemed to return good results for all samples other than VA15 which had errors comparable to the returned values of k . This was because VA15 showed a higher and less discrete degree of inhomogeneity relative to the other samples, making it difficult to categorise its particles into distinct groups. All samples appeared to show their particles distributed about a modal k value, with samples VA11, VA19 and VA5 appearing to show the development of a secondary mode of more highly absorbing particles. This distribution was due to the varied make-up of particles within the sample, with the vitric and crystalline particles showing substantially less absorption than the lithic particles. A better idea of the true distributions, as well as a more accurate overall value, would have been gained with a larger sample size.

The variation in the overall real and imaginary part of the refractive index between the samples would have been primarily due to their differing chemical compositions, determined by the type of eruption from which they originate [6]. A key ingredient of volcanic matter is silica (SiO_2). Both real and imaginary parts were shown to correlate with percentage silica content of the ash (see Appendix C).

A substantial limitation of the particle absorption method was that it was unable to test the particles with a size parameter lower than about 120 due to the restrictions mentioned in Section

2.2 and the sensitivity of the camera. These particles, although individually small, constitute a large combined volume within each sample. Furthermore, there is evidence that smaller aerosol particles are more highly absorbing [22], meaning that the returned overall k values would be smaller than the true values for the entirety of the samples.

The overall k values were calculated by volume-averaging the values for the individual, constituent particles which is a commonly employed procedure and allowed for the straight forward combination of all the unique, measured particles. However, there has been some debate as to whether this is an effective approach when applied to atmospheric aerosols [15, 23, 24], and it has been suggested that the Bruggeman and Maxwell Garnett mixing rules may map the individual particle's refractive indices to that of the bulk matter more honestly [25]. It would be interesting to see how different the results would have been had these rules been applied but the lengthy calculations would have been unlikely to have made a significant difference due to the comparatively narrow range of k values of the particles that were retrieved.

The averaging procedure required the assumption that the ashes were an external mixture of particles, each of a uniform consistency. However, fragments were often either fused from a mixture of different materials or contained bubbles of volcanic gas. These inhomogeneities within the particles themselves would have produced unaccounted for scattering, which would have been assumed to be absorption, and would have led to inaccurately high values for k .

6 Conclusions and suggestions for further research

The real part of the refractive index of ten volcanic ash samples was successfully determined. A new method to determine the imaginary part of the refractive index was developed and successfully implemented to retrieve the imaginary part of the refractive index of six of these samples. This report provides a way to extract much needed volcanic ash optical data, with inexpensive and accessible equipment. The obtained results could be used to better interpret satellite images of the eruptions from which they come or other eruptions with plumes containing similar ash.

Although apparently effective, the true success

of the particle absorption method cannot be gauged until a calibration material has been tested. Coloured glass has been suggested as a material which would provide a known value of the complex refractive index to test the method against.

To test the absorption of small particles, the samples could be filtered so that only the finest particles remain. They could then be suspended in a liquid of a matched refractive index and the extinction could be measured. Providing they are small enough, the Raleigh approximation would mean that extinction would be entirely due to absorption, and the imaginary part of the refractive index could be retrieved and compared to that of the larger particles measured in this project.

7 Acknowledgements

My heartfelt thanks go Don Grainger and Ben Reed for the assistance and advice given throughout the project. Thanks must also go to Karen Applin and Keith Long for their patience during my use of the microscope in the teaching labs.

References

- [1] Horwell, C. J. and Baxter, P. J., The respiratory health hazards of volcanic ash: a review for volcanic risk mitigation, *Bulletin on Volcanology*, v. 69, p. 1-24, 2006.
- [2] International Civil Aviation Organisation, *Manual on Volcanic Ash, Radioactive Material and Toxic Chemical Clouds*, ICAO Doc 9691, 2007.
- [3] Robock, A., Volcanic eruptions and climate, *Reviews of Geophysics*, v. 38.2, p. 191-219.
- [4] Grainger, R. G., Peters, D. M., Thomas, G. E., Smith, A. J. A., Siddans, R., Carboni, E. and Dudhia A., Measuring volcanic plume and ash properties from space, Pyle, D. M., Mather, T. A. and Biggs, J. (eds.), *Remote Sensing of Volcanoes and Volcanic Processes: Integrating Observation and Modelling*, Geological Society of London Special Publications, v. 380, p. 293-320, 2013.
- [5] Schmid, R., Descriptive nomenclature and classification of pyroclastic deposits and fragments: Recommendations of the IUGS Sub-

- commission on the Systematics of Igneous Rocks, *Geology*, v. 9, p.41-43, 1981.
- [6] Heiken, G., Wohletz, K. H., *Volcanic ash*, University of California Press, 1985
- [7] Patterson, E. M., Measurements of the imaginary part of the refractive index between 300 and 700 nanometers for Mount St. Helens ash, *Science*, v. 211, p. 836-838, 1981.
- [8] Patterson, E. M., Pollard, C. O. and Galindo, I., Optical-properties of the ashes from El-Chichon volcano, *Geophysical Research Letters*, v. 10, p. 317-320, 1983.
- [9] Patterson, E. M., Optical absorption coefficients of soil-aerosol particles and volcanic ash between 1 and 16 μm , *Proceedings of the Second Conference on Atmospheric Radiation*, American Meteorological Society, Washington DC, p. 177–180, 1994.
- [10] Krotkov, N. A., Flittner, D. E., Krueger, A. J., Kostinski, A., Riley, C., Rose, W. and Torres, O., Effect of particle non-sphericity on satellite monitoring of drifting volcanic ash clouds, *Journal of Quantitative Spectroscopy and Radiative Transfer*, v. 63, p. 613-630, 1999.
- [11] Pollack, J. B., Toon, O. B. and Khare, B. N., Optical properties of some terrestrial rocks and glasses, *Icarus*, v. 19, p. 372-389, 1973.
- [12] Egan, W., Hilgeman, T. and Pang, K., Ultraviolet complex refractive-index of Martian dust – Laboratory measurements of terrestrial analogs, *Icarus*, v. 25, p. 344-355, 1975.
- [13] Volz, F. E., Infrared optical constants of ammonium sulfate, Sahara dust, volcanic pumice and flyash, *Applied Optics*, v. 12, p. 564-568, 1973.
- [14] Toon, O. B., Pollack, J. B. and Sagan, C., Physical properties of the particles composing the Martian dust storm of 1971–1972, *Icarus*, v. 30, p. 663-696, 1977.
- [15] Bohren, C. F., Huffman, D. R., *Absorption and Scattering of Light by Small Particles*, New York, Chichester: Wiley, 1983.
- [16] Grainger, R. G., Lucas, J., Thomas, G. E., and Graham B. L. Ewen, G. B. L., Calculation of Mie derivatives, *Optical Society of America*, 2004.
- [17] Francis, P. N., Cooke, M. C. and Saunders, R., Retrieval of physical properties of volcanic ash using Meteosat: A case study from the 2010 Eyjafjallajökull eruption, *Journal of Geophysical Research*, v. 117, i. 20, p. D00U09, 2012.
- [18] Mishchenko, M. I., Travis, L. D. and Lacis, A. A., *Scattering, absorption, and emission of light by small particles*, Cambridge : Cambridge University Press, 2002.
- [19] Nesse, W. D., *Introduction to optical mineralogy*, New York, Oxford: Oxford University Press, 1991.
- [20] Zimanowski, B., Wohletz, K., Dellino, P., Büttner, R., The volcanic ash problem, *Journal of Volcanology and Geothermal Research*, v. 122, i. 1-2, p. 1-5, 2003.
- [21] Ebert, M., Weinbruch, S., Rausch, A., Gorzawski, G., Hoffmann, P., Wex, H., and Helas, G., Complex refractive index of aerosols during LACE 98 as derived from the analysis of individual particles, *Journal of Geophysical Research*, v. 107, i. 20, p. LAC 3-1–LAC 3-16, 2002.
- [22] Lindberg, J. D. and Gillespie, J. B., Relationship between particle size and imaginary refractive index in atmospheric dust, *Applied Optics*, v. 16, i. 10, p. 2628-2630, 1977.
- [23] Gillespie, J. B., Jennings, S. G. and Lindberg, J. D., Use of an average complex refractive index in atmospheric propagation calculations, *Applied Optics*, v. 17, i. 7, p. 989-991, 1978.
- [24] Lindberg, J. D., The composition and optical absorption coefficient of atmospheric particulate matter, *Optical and Quantum Electronics*, v. 7, p.131-139, 1975.
- [25] Chylek, P., Srivastava, V., Pinnick, R. G. and Wang, R. T., Scattering of electromagnetic waves by composite spherical particles:

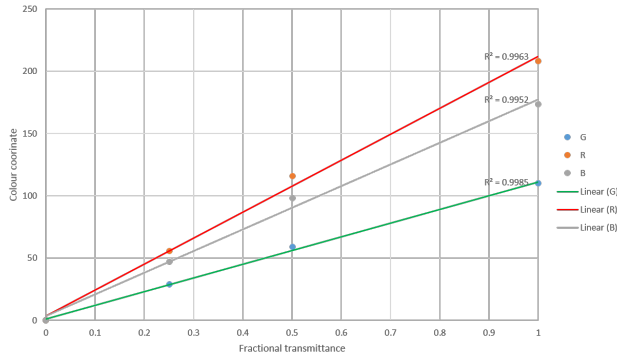
experiment and effective medium approximations, *Applied Optics*, v. 27, i.12, p2396-2403, 1988.

C. Plots of real and imaginary refractive index against SiO₂ % composition

(See next page)

Appendices

A. Camera calibration graph



The lines show a linear relationship between the RGB coordinates and fractional transmittance, $T = 10^{-d}$, where d is optical density.

B. Determining the errors in the overall k values

For n uncorrelated observations with standard deviations σ_i and weights w_i , the weighted sample mean has standard deviation:

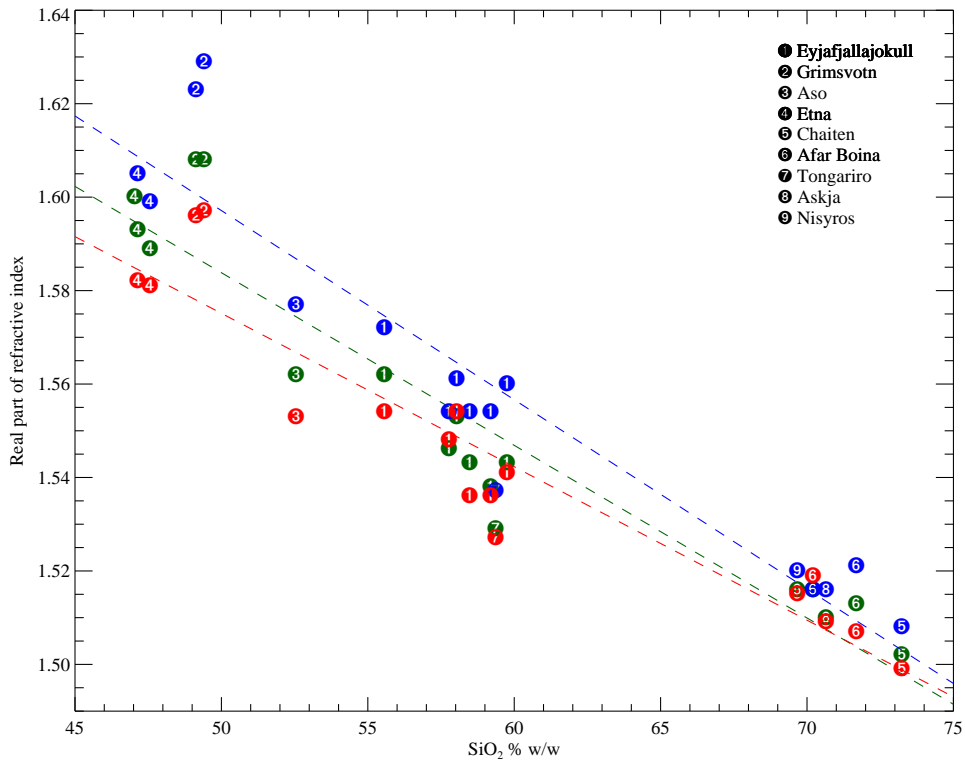
$$\sigma(\bar{x}) = \sqrt{\sum_{i=1}^n w_i^2 \sigma_i^2}$$

The 30 particles in were catagorised into three distinct groups (clear, lithic and mixed) and the standard deviation within each group was calculated (σ_c , σ_l and σ_m).

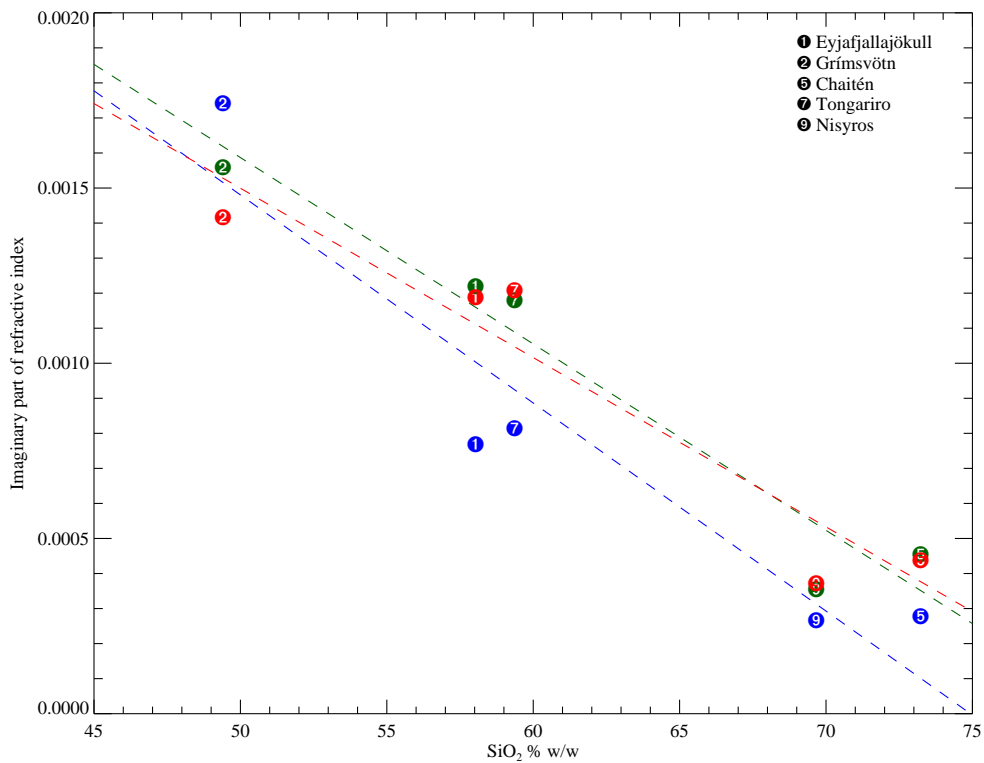
The weight of a particle was given by its volume over the sum of all the volumes of the particles in the sample:

$$w_i = \frac{V_i}{\sum_{n=1}^{30} V_n}$$

With each particle having a weight set by its volume and a standard deviation given by its group designation, the standard deviation of the weighted mean could be calculated.



The real parts of the refractive indices of some of ashes studied against their measured SiO_2 % composition. Plot: Ben Reed (Atmospheric, Oceanic and Planetary Physics, Oxford) ; Composition data: Gemma Prata (Earth Sciences, Oxford).



The imaginary parts of the refractive indices of some of ashes studied against their measured SiO_2 % composition. Plot: Ben Reed (Atmospheric, Oceanic and Planetary Physics, Oxford); Composition data: Gemma Prata (Earth Sciences, Oxford).